International Journal of Science and Engineering Applications
Volume 15-Issue 07, 44 – 51, 2026, ISSN:- 2319 - 7560
DOI: 10.7753/IJSEA1507.1008

Sliding Mode Manifold Oriented Adaptive PID Fusion Control Strategy with Dynamic Weight Distribution

Shengyi Zhang
Yangtze University
School of Electronic Information and Electrical Engineering
Jingzhou, China

Abstract:To address the trade-off between transient response and steady-state precision in single-phase full-bridge inverters, this paper proposes an adaptive Proportional-Integral-Derivative (PID) fusion control strategy based on manifold-oriented dynamic weight allocation. This paper proposes an adaptive PID fusion control strategy based on manifold-oriented dynamic weight allocation. The strategy integrates a double-closed-loop PID controller and a sliding mode controller (SMC) using a nonlinear mapping guided by the sliding mode manifold. By dynamically balancing these control laws, the strategy effectively reduces overshoot to 0.12%, a common issue in linear control, while also suppressing steady-state chattering and harmonic distortion typical of standalone SMC. The system's stability is rigorously verified using Lyapunov theory. Simulation results demonstrate that the fusion strategy effectively suppresses startup overshoot, reducing it to 0.12%, compared to 1.7 V in conventional PID control. Under steady-state conditions, the proposed method maintains an error envelope of 0.4V and reduces Total Harmonic Distortion (THD) to 1.32%, compared to 4.44% for PID and 3.80% for SMC. Furthermore, the strategy exhibits superior disturbance rejection during load mutations, ensuring high waveform quality and rapid dynamic recovery. This framework effectively couples the high-gain robustness of nonlinear control with the high-precision smoothing of linear control, providing an optimized, theoretically rigorous solution for high-performance power quality control in inverter applications.

Keywords: single-phase full-bridge inverter；sliding mode control；adaptive PID；dynamic weight allocation；SPWM

1. Introduction

With the extensive application of power electronics technology in microgrids, aerospace[1][2], and electric vehicles[3], the high-performance control of DC-AC inverters[4][5] has emerged as a focal point of academic interest[6][7]. Such systems are characterized by typical nonlinearity, time-varying behavior, and sensitivity to parameter fluctuations[8]. Traditional double-closed-loop PID control, known for its simplicity and maturity, has been widely used in industrial applications[9][10]. However, linear PID controllers are designed for small-signal models. When faced with nonlinear disturbances, such as large load jumps or input voltage fluctuations, they struggle to balance transient response and steady-state stability, which may lead to system instability.[11][12]. This paper specifically focuses on single-phase full-bridge inverters.

To address the limitations of linear control, sliding mode control has been introduced as a highly robust nonlinear control method. SMC enforces the system state to follow a predetermined trajectory through a preset switching manifold[13][14], demonstrating high immunity to model uncertainties. Nevertheless, its inherent "chattering" issue not only increases switching losses but may also induce high-frequency parasitic modes in the system, thereby limiting its direct application in refined power conversion scenarios[15][16][17].

In recent years, researchers have begun to investigate fusion algorithms that combine the stability of PID with the dynamic performance of SMC[18][19]. Traditional composite control often employs fixed-gain switching, which is prone to generating secondary disturbances at switching points[20][20]. This paper proposes a dynamic weight distribution adaptive PID fusion control strategy guided by sliding mode manifolds. The core of this strategy lies in utilizing the sliding mode surface function s(t) as an evaluation metric to dynamically perceive the degree of system state deviation from the equilibrium point. During dynamic processes far from the equilibrium point, the weight of sliding mode control is increased to enhance convergence speed. As the system approaches the equilibrium point in steady-state processes, an adaptive mechanism smoothly transitions to a PID-dominant mode, leveraging integral action to eliminate residual static errors. This approach aims to achieve complementary advantages between nonlinear sliding mode control and adaptive PID regulation. Finally, the single control algorithm and the fusion algorithm are quantitatively evaluated from the perspectives of parameter improvement dimensions and waveform observable indices, thereby demonstrating the superiority of the fusion control algorithm.

2. Material and Methods

2.1 Individual control algorithm design

The full bridge inverter system topology is illustrated in Fig. 1, where the components of the system are shown clearlyFig 1 Single phase full bridge inverter circuit topology. The system consists of a DC input source, a full-bridge inverter circuit, an output LC filter, and a load module. This topology is designed to convert the DC voltage V_{dc} into a stable sinusoidal AC voltage, which can supply the rear load.

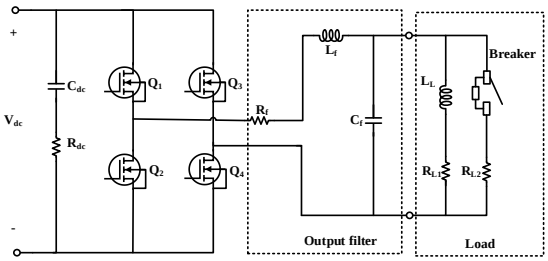

Fig 1 Single phase full bridge inverter circuit topology

The DC bus side contains a DC voltage source V_{dc} and a supporting capacitor link composed of a capacitor C_{dc} and

International Journal of Science and Engineering Applications
Volume 15-Issue 07, 44 – 51, 2026, ISSN:- 2319 - 7560
DOI: 10.7753/IJSEA1507.1008

an equivalent series resistance R_{dc} to suppress bus voltage fluctuations. The full-bridge inverter consists of power switches Q1-Q4 and converts voltage using unipolar SPWM modulation. The output filtering link uses a second-order low-pass filter composed of filter inductance L_f, inductance equivalent resistance R_f and filter capacitor C_f to filter out high-frequency switch burrs and make the output waveform smooth and sinusoidal. The load module is specially designed with switchable load, which is composed of fixed resistive inductive load L_L, R_{L1} and switching resistor R_{L2} controlled by the circuit breaker to verify the dynamic response capability and robustness of the control algorithm under sudden load increase/decrease conditions.

According to Kirchhoff's law (KVL/KCL), the state space model of the inverter in the continuous conduction mode is established by ignoring the switching loss:

$$\begin{cases} L_i \dfrac{di_L}{dt} = uV_{dc} - i_L R_i - v_o \\ C_i \dfrac{dv_o}{dt} = i_L - i_o \end{cases} \quad (1)$$

Where $u \in \{-1,1\}$ is the control function control law, v_o is the output voltage, i_o is the output current of the load terminal, i_L is the inductance current.

2.1.1 *Double closed-loop PID control*

To accurately track the inverter output voltage, this paper employs a double-closed-loop control architecture with a voltage outer loop and a current inner loop (Fig. 2) for steady-state error comparison. In this architecture, the outer voltage loop is responsible for maintaining the stability of the output voltage v_o and tracking the reference signal V_{ref} ; The inner current loop takes the inductive current i_L as the controlled object to enhance the anti-interference ability of the system and realize overcurrent protection.

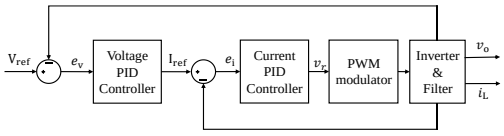

Fig 2 Double closed-loop PID control architecture

Where e_v is the voltage error, e_i is the current error, and v_r is the output modulation reference signal.

a) Voltage outer loop design

The difference between the reference voltage V_{ref} and the feedback voltage v_o is taken as the voltage outer loop input, and the output is taken as the reference instruction I_{ref} of the inductance current through the voltage PID controller.

The voltage error is defined as $e_v = V_{ref} - v_o$. After passing through the voltage loop controller, the reference value of inductance current generated is:

$$i_{ref} = K_{pv}e_v + K_{iv}\int e_v dt + K_{dv}\frac{de_v}{dt} \quad (2)$$

Where K_{pv} is the proportional coefficient, K_{iv} is the integral coefficient, and K_{dv} is the differential coefficient.

The command value is then sent to the inner ring as the current setting signal.

b) Current inner ring design

The difference between I_{ref} given by the outer loop and the measured inductance current i_L is taken as the input of the current inner loop, and the modulated wave voltage command is output through the current PID controller.

The inner current loop tracks the inductance current to speed up the system's response to load disturbances. The current error $e_i = I_{ref} - i_L$ is regulated by the current loop controller $G_i(s)$, and the modulation reference signal v_r is output:

$$v_r = G_i(s) \cdot e_i \quad (3)$$

In this model, the output modulation reference signal v_r is input into the PWM generator after gain.

Using the pole assignment method, according to the main circuit parameters and the definition of non dominant poles, the non dominant pole correlation $m = 8, n = 10$, expected dynamic performance, damping coefficient $\xi = 7$, and natural frequency $\omega = 2500 rad/s$ are taken. $K_{pv} = 0.075, K_{iv} = 135.8, K_{dv} = 0.1$, $K_{pv} = 0.27, K_{iv} = 1852.1, K_{dv} = 0.1$ can be obtained.

The transfer function of voltage regulator and current regulator is:

$$G_v(s) = 0.075 + \frac{135.8}{s} + 0.1s \quad (4)$$

$$G_i(s) = 0.27 + \frac{1852.1}{s} + 0.1s \quad (5)$$

2.1.2 *Sliding mode control*

In order to achieve the fast dynamic response of the inverter output voltage system, this paper uses a typical sliding mode control architecture (Fig 3) as a dynamic response comparison test. The state variables are defined as inductance current i_L and output voltage v_o. u_{eq} is the equiv.alent control, u_n is the reaching law control, and $u \in [-1,1]$ is the continuous duty cycle signal of the final control input.

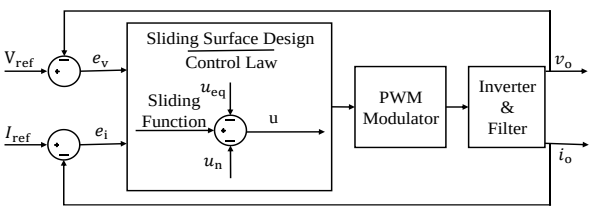

International Journal of Science and Engineering Applications
Volume 15-Issue 07, 44 – 51, 2026, ISSN:- 2319 - 7560
DOI: 10.7753/IJSEA1507.1008

Fig 3 Sliding mode control architecture

a) Sliding surface design

In order to realize the accurate tracking of voltage and the rapid response of current simultaneously, a linear sliding mode surface s integrating voltage and current errors is constructed in this paper. The voltage error $e_v = v_o - V_{ref}$ and current error $e_i = i_L - I_{ref}$ are defined. The sliding mode function is designed as follows:

$$s = e_i + \beta e_v \quad (6)$$

Where, β is the sliding mode surface weight coefficient, which is used to adjust the weight relationship between voltage tracking performance and current stability. In order to achieve complete decoupling tracking, the reference current I_{ref} is derived based on the capacitance current equation:

$$I_{ref} = \frac{V_{ref}}{R_L} + C_f \frac{dV_{ref}}{dt} \quad (7)$$

The reference current not only includes the load consumption, but also compensates the capacitor charging and discharging current required by the voltage change.

b) Derivation of control law and equivalent control

The sliding mode control law consists of equivalent control u_{eq} and reaching law control u_n.

When the system enters sliding mode, $s = 0$ and $\dot{s} = 0$ are met. Derive the sliding surface s and substitute it into the state equation:

$$\dot{s} = \frac{1}{L_f}(uV_{dc} - i_f R_f - v_o) - \frac{dI_{ref}}{dt} + \beta\left(\frac{i_L - i_o}{C_f} - \frac{dV_{ref}}{dt}\right) = 0 \quad (8)$$

Solve the equivalent control term u_{eq} :

$$u_{eq} = \frac{L_f}{V_{dc}}\left[\frac{R_f i_L + v_o}{L_f} + \frac{dI_{ref}}{dt} - \beta\left(\frac{i_L - i_o}{C_f} - \frac{dV_{ref}}{dt}\right)\right] \quad (9)$$

c) Approach Law and Buffeting Suppression

In order to ensure that the system approaches the sliding mode surface from any initial state in a finite time and reduce the "chattering" phenomenon caused by control law switching, this paper introduces the saturation function $sat(\frac{s}{\Delta})$ with boundary layer instead of the traditional symbolic function $\mathrm{sgn}(s)$.

The final control output u is expressed as:

$$u = -\frac{A \cdot L_f}{V_{dc}} - K \cdot sat\left(\frac{s}{\Delta}\right) \quad (10)$$

Where, A is the combination term related to the system equivalent control, Δ is the boundary layer thickness, and K is the approach gain.

Natural evolution term A of system state:

$$A = -\frac{R_f i_L + v_o}{L_f} - \frac{dI_{ref}}{dt} + \beta\left(\frac{i_L - i_o}{C_f} - \frac{dV_{ref}}{dt}\right) \quad (11)$$

The expression of saturation function is:

$$sat\left(\frac{s}{\Delta}\right) = \begin{cases} \frac{s}{\Delta}, & |s| \le \Delta \\ \mathrm{sgn}(s), & |s| > \Delta \end{cases} \quad (12)$$

The system has fast approaching characteristics outside the boundary layer, and it can be converted into linear regulation within the boundary layer, which can effectively suppress high-frequency switching pulsation.

2.2 Adaptive PID fusion control with dynamic weight distribution based on sliding mode manifold guidance

First, the second-order average model of single-phase full bridge inverter is considered. Let v_o and i_L be output voltage and inductance current respectively, and the state space equation of the system can be expressed as:

$$\begin{bmatrix} \dot{v}_o \\ \dot{i}_L \end{bmatrix} = \begin{bmatrix} 0 & \frac{1}{C_f} \\ -\frac{1}{L_f} & -\frac{R_f}{L_f} \end{bmatrix} \begin{bmatrix} v_o \\ i_L \end{bmatrix} + \begin{bmatrix} 0 \\ \frac{V_{dc}}{L_f} \end{bmatrix} u - \begin{bmatrix} \frac{1}{C_f} \\ 0 \end{bmatrix} i_o \quad (13)$$

Among them u Is the modulation ratio. All parameters are consistent with Experiment 2.1, and the voltage tracking error $e(t) = V_{ref}(t) - v_o(t)$ is defined. The fusion control quantity proposed in this paper can be expressed as:

$$u = \alpha(|s|)d_{sm} + [1 - \alpha(|s|)]u_{pid} \quad (14)$$

In order to realize the smooth connection between the high robustness of sliding mode control (SMC) and the high steady-state accuracy of adaptive PID control, this paper designs an exponential mapping nonlinear dynamic weight factor $\alpha(|s|)$ based on the manifold offset degree, whose mathematical expression is defined as:

$$\alpha(|s|) = 1 - e^{-\kappa|s|^n} (\kappa > 0, n \ge 1) \quad (15)$$

Where, $|s|$ is the Euclidean distance between the current system state and the sliding mode manifold; κ is the convergence regulation coefficient, which determines the sensitivity of control weight switching between SMC and PID; n is the shape factor ($n = 1$ is taken in this paper).

The selection logic of this function is based on the following three physical evolution mechanisms:

Global C^∞ continuity: Compared with piecewise linear functions, exponential mapping is infinitely derivable in the full domain. This ensures the smoothness of the control quantity u in the process of approaching, effectively suppresses the control law step caused by hard switching, and thus reduces the instantaneous burr of the inverter output voltage.

International Journal of Science and Engineering Applications
Volume 15-Issue 07, 44 – 51, 2026, ISSN:- 2319 - 7560
DOI: 10.7753/IJSEA1507.1008

Error manifold guidance: when the system is subject to a large disturbance or the load suddenly deviates from the manifold ($|s|\neq 0$), $\alpha(|s|)\to 1$, the control law is dominated by SMC, and its strong nonlinear gain is used to ensure rapid regression of the system state. With the error convergence ($|s|\to 0$), $\alpha(|s|)$ decays exponentially to 0, and PID gain gradually dominates. The integral effect is used to compensate the residual static error in the sliding mode boundary layer.

Decoupling design principle: through the tuning of κ, the "fast approaching zone" and "high precision steady state zone" of the system can be decoupled. According to the boundary layer thickness Δ, set $|s|=\Delta$ at $\alpha\geq 0.95$, and then deduce $\kappa\geq -\frac{\ln(0.05)}{\Delta}$.

The fusion control flow chart is shown in Fig 4:

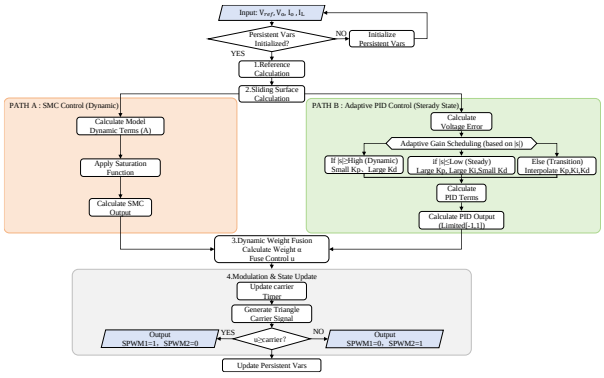

Fig 4 Fusion Control Flow Chart

2.2.1 Frequency domain analysis of adaptive PID controller

In order to quantitatively analyze the performance of adaptive PID under different operating conditions, Laplace transform is introduced. s is defined as a sliding surface function (to avoid confusion, this section uses σ to represent the sliding surface and s to represent the complex frequency variable). The general transfer function of voltage loop adaptive PID is:

$$G_{pid}(s,|\sigma|)=K_p(|\sigma|)+\frac{K_i(|\sigma|)}{s}+K_d(|\sigma|) \quad (16)$$

Where K_p is the proportional coefficient, K_i is the integral coefficient, and K_d is the differential coefficient. In order to ensure fairness, the basic coefficients are still consistent with the 2.1 double closed-loop parameters in this experiment.

According to the control logic, the system is divided into three typical working intervals:

a) Steady state precision zone ($|\sigma|\leq\sigma_{low}$)

In this interval, the system approaches the equilibrium point, and the control goal is to eliminate the static error. According to the root locus analysis of the closed-loop characteristic equation, the proportional gain multiplier has the best damping ratio at 1.6 times. According to the control law, the remaining parameters are:

$$\begin{aligned} K_p &= 1.6K_{p\_base} \\ K_i &= 2.0K_{i\_base} \\ K_d &= 0.25K_{d\_base} \end{aligned} \quad (17)$$

Its transfer function is:

$$G_{ss}(s)=\frac{0.25K_{d\_base}s^2+1.6K_{p\_base}s+2.0K_{i\_base}}{s} \quad (18)$$

$G_{ss}(s)$ in this range has extremely high low-frequency gain (provided by $\frac{2.0K_{i\_base}}{s}$), which ensures that the system tracks the fundamental reference signal without static error. At the same time, the lower differential gain weakens the negative effect of high-frequency noise on the THD of steady waveform.

b) Transient disturbance area ($|\sigma|\geq\sigma_{high}$)

When load sudden change causes $|\sigma|$ surge, the system enters into strong robust mode. Through the root locus analysis of the closed-loop characteristic equation, the parameter values are :

$$\begin{aligned} K_p &= 0.25K_{p\_base} \\ K_i &= 0 \\ K_d &= 2.2K_{d\_base} \end{aligned} \quad (19)$$

Its transfer function degenerates to PD controller:

$$G_{tr}(s)=0.25K_{p\_base}+2.2K_{d\_base}s \quad (20)$$

At this time, $K_i=0$ completely solved the problem of integral saturation under large signal disturbance. The high differential gain $2.2K_{d\_base}$ introduces a leading zero point in the open loop transfer function of the system, which significantly improves the phase margin of the system, thus suppressing the transient oscillation caused by SMC.

c) Parameter transition area ($\sigma_{low}<|\sigma|<\sigma_{high}$)

In this interval, the parameter evolves linearly with $|\sigma|$. Let $\lambda=\frac{\sigma_{high}-|\sigma|}{\sigma_{high}-\sigma_{low}}$ (where $\lambda\in[0,1]$), then the adaptive transfer function can be expressed as:

$$G_{mid}(s,\lambda)=K_p(\lambda)+\frac{K_i(\lambda)}{s}+K_d(\lambda)s \quad (21)$$

The smooth transition of the parameters ensures the energy continuity of the control rights within the PID and between the PID and SMC, and avoids the secondary voltage distortion caused by the control law switching.

2.2.2 Closed-loop stability evaluation of fusion strategy

To rigorously verify the stability of the proposed adaptive PID fusion control strategy, we utilize Lyapunov stability theory. This ensures that the system remains Uniformly Ultimately Bounded (UUB) under the fusion control law. Lyapunov functions are widely used to establish the stability of

nonlinear systems and provide insights into the system's convergence behavior over time.

a) Lyapunov Candidate Function Definition

The Lyapunov candidate function $V(s,e_i)$ is defined as:

$$V(s,e_i)=\frac{1}{2}s^2+\frac{1}{2\gamma}2e_i^2 \quad (22)$$

where: s is the sliding surface (sliding mode state), e_i represents the integral error in the PID controller, γ is a constant that ensures the influence of the integral error term.

The role of this Lyapunov function is to analyze whether the system's state remains stable under the influence of disturbances or whether it will ultimately stabilize within a certain bound.

b) Time Derivative of the Lyapunov Function

Taking the time derivative of the Lyapunov candidate function, we get:

$$\dot{V}(s,e_i)=s\cdot\dot{s}+\frac{1}{\gamma}e_i\cdot\dot{e}_i \quad (23)$$

Where $\dot{s}$ is the rate of change of the sliding surface state and $\dot{e}_i$ is the error dynamics of the PID control. The system's control law is composed of a weighted combination of sliding mode control (SMC) and adaptive PID control, so we can express the control law as:

$$u(t)=w(s)\cdot u_{SMC}+(1-w(s))\cdot u_{PID} \quad (24)$$

where $w(s)$ is the dynamic weight factor defined based on the deviation from the sliding mode manifold.

c) Effect of System Disturbances

Assume the system is subjected to disturbances $d(t)$, with the bound:

$$|d(t)|\le d_{max} \quad (25)$$

The presence of disturbances may impact the system's convergence and stability, but we will show how, under the control law design, the system can still guarantee stability despite the disturbances.

d) Introduction of Control Law and Stability Conditions

The sliding mode control term u_{SMC} and the PID control term u_{PID} are designed to optimize the system's fast dynamic response and steady-state accuracy, respectively. When the system is in the sliding mode, the sliding mode control dominates, ensuring a fast response to disturbances. As the system gradually approaches the steady state, the PID control takes over and eliminates the static error.

After combining the control laws, the time derivative of the Lyapunov function becomes:

$$\dot{V}(s,e_i)=s\cdot\left(-k\cdot sat\left(\frac{s}{\phi}\right)\right)+\frac{1}{\gamma}e_i\cdot e \quad (26)$$

Where k is the gain of the sliding mode control, ϕ is the boundary layer thickness, and $sat(x)$ is the saturation function. The design of the sliding mode control ensures that the system will approach the desired trajectory, while limiting the high-frequency chattering caused by control switching.

e) Final Derivation: Uniform Ultimate Boundedness (UUB)

Under the control law, when the system is far from equilibrium, the sliding mode control dominates the system behavior, and the system state converges quickly. However, as the system approaches steady state, PID control gradually takes over, compensating for the static error.

In the presence of disturbances, the time derivative of the Lyapunov function satisfies:

$$\dot{V}(s,e_i)\le -k|s|+|s|d_{max}+\frac{1}{\gamma}|e_i||e| \quad (27)$$

If the control gain k satisfies the following condition:

$$k>d_{max} \quad (28)$$

then the time derivative of the Lyapunov function becomes:

$$\dot{V}(s,e_i)\le -\eta|s|+bounded\ terms \quad (29)$$

Thus, we can conclude that when the control gain k exceeds the disturbance bound, the system state will remain uniformly ultimately bounded (UUB), meaning:

$$\lim_{t\to\infty}|s(t)|\le \text{ò} \quad (30)$$

This shows that, through the dynamic weight switching, the system not only maintains global stability but also rapidly recovers from disturbances and stabilizes at the desired steady state.

f) Conclusion

Through the Lyapunov stability analysis presented above, we prove that the proposed adaptive PID fusion control strategy ensures Uniform Ultimate Boundedness (UUB) of the system under the influence of disturbances and load variations. Therefore, the designed control strategy guarantees system stability and provides robust performance in practical applications.

When the system is in the approaching steady state stage ($|s|\to 0$, $\alpha\to 0$): at this time, the control law is dominated by the adaptive PID, $u\approx u_{pid}$. According to the structure of the adaptive PID, when the system enters the linear region near the sliding mode surface, the root of the characteristic equation of the error system is located in the left half complex plane by adjusting K_p,K_i,K_d . At this time, $\dot{s}$ is forced to converge to $s=0$, and the integral term $\tilde{\xi}$ of PID eliminates the static error.

In order to ensure global stability, the switching gain K_{smc} in the control law must meet the upper limit constraint of disturbance:

$$K_{smc}>\frac{L_f}{V_{dc}}|A_{\max}| \quad (31)$$

According to Lyapunov stability theorem:

① $V(s,\tilde{\xi})$ is positive definite.

International Journal of Science and Engineering Applications
Volume 15-Issue 07, 44 – 51, 2026, ISSN:- 2319 - 7560
DOI: 10.7753/IJSEA1507.1008

②Under the action of fusion control law, $\dot{V} = s[A + \frac{V_{dc}}{L_f}(\alpha d_{sm} + (1-\alpha)u_{pid})] + \ldots$ can guarantee $\dot{V} \le 0$ in the full definition domain through smooth switching of dynamic weight α.

③When and only when $s = 0$ and the error is 0, $\dot{V} = 0$.

Conclusion: The system is asymptotically stable under the sliding mode manifold oriented dynamic weight control, and meets the accessibility condition $s\dot{s} < 0$.

Micro gain analysis

Considering the weighting factor $\alpha(|\sigma|)$, the total control gain $G_{total}(s)$ of the system is the weighted sum of the sliding mode nonlinear gain and the PID linear gain. The micro gain analysis near the sliding mode surface shows that by dynamically adjusting K_d, the equivalent damping ratio ζ of the fusion strategy at sliding mode surface $\sigma = 0$ meets:

$$\zeta \propto \sqrt{\frac{(1-\alpha)K_d + \beta_s C_f}{L_f}} \quad (32)$$

This proves that by increasing K_d when $|\sigma|$ is large, the high-frequency fluctuation caused by SMC can be effectively compensated to achieve better dynamic attenuation characteristics.

3. Results and discussion

The comparative analysis of output voltage error waveforms for the three control algorithms is depicted in Fig 5. he green waveform represents double-closed-loop PID control, a conventional method. During startup, the voltage error exhibits significant overshoot, with a peak error of approximately 1.7 V. Compared to the maximum fluctuation error of 0.5 V at steady state, the startup impact is notably pronounced. When the load is halved at 0.1s and restored at 0.2s, the erPID demonstrates minimal fluctuation, with a very narrow envelope, indicating good steady-state smoothness of the model. The blue waveform, corresponding to sliding mode control, demonstrates excellent disturbance rejection capability, as no significant transient deviation is observed during load switching. However, due to inherent chattering effects, the steady-state error exhibits noticeable oscillations, with an amplitude of approximately 0.7 V. This indicates that while SMC ensures fast dynamic response, it compromises steady-state waveform quality.

In comparison, the red waveform (fusion control) exhibits significantly reduced overshoot during startup, with a maximum value of approximately 0.12%, indicating effective transient suppression compared to PID control.. Once the system rapidly attains a steady state, the voltage error signal remains confined within a minimal range, with a 0.4V sinusoidal error curve observed during steady-state conditions. During load switching at 0.1s and 0.2s, the voltage error demonstrates no significant elevation or reduction, while the amplitude and frequency of the output voltage maintain a high degree of stability. The model combines the precision of linear control with the robustness of nonlinear control, preserving waveform purity in the steady-state phase.

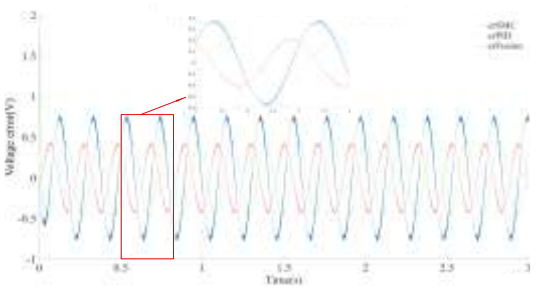

Fig 5 Comparison of output voltage error waveforms of three control methods

Fig 6 shows the harmonic spectrum distribution of the three models under 50Hz fundamental working condition. Since the load is resistive-inductive, current THD is used as an indirect indicator of voltage quality. The total harmonic distortion test results of double loop PID control, sliding mode control and fusion control are 4.44%, 3.80% and 1.32% respectively. Obviously, the THD of fusion control is smaller, and all three meet the general requirements of national power quality.

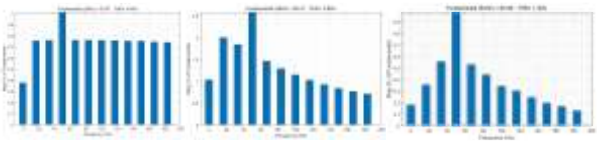

Fig 6 THD Analysis of Output Current of Three Models

Comprehensive observability waveform and parameter comparison, as shown in Table 1, sliding mode manifold oriented dynamic weight distribution adaptive PID fusion control is superior to single control in response time, steady-state maximum error, current and power quality, overshoot and robustness.

Table 1 Comparison of performance parameters of three control models

Parameter	PID	SMC	Fusion Control
response time	1T	1T	0.5T
Maximum steady-state error	0.5V	0.7V	0.4V
Current THD	4.44%	3.80%	1.32%
Overshoot	0.16%	0.25%	0.12%
Robustness	average	strong	strong

For the problem of steady-state error, it can be optimized from two aspects: a more optimal parameter model can be deduced using intelligent algorithms; Find better mapping nonlinear dynamic weighting factors. These measures can effectively reduce the steady-state maximum error, and can improve the response speed and stability of the fusion algorithm control.

4. Conclusion

This study demonstrates that the manifold-oriented adaptive PID fusion control strategy, based on the sliding mode surface and dynamic weight distribution, outperforms single control methods in single-phase full-bridge inverter control. It has been proven that fusion control can integrate the strengths of both algorithms, offering promising prospects and suggesting the potential for dynamically fusing different algorithms.

At the level of co-evolutionary mechanisms, this strategy transcends the limitations of traditional control methods. By

leveraging the high nonlinear gain of sliding mode control, it ensures robust system performance under significant disturbances. Simultaneously, the integration of the integral effect from adaptive PID significantly mitigates the inherent steady-state chattering and static error associated with sliding mode control. Simulation results indicate that, in comparison to a single SMC approach, the fusion control strategy not only maintains rapid dynamic response but also substantially enhances the quality of steady-state waveforms, with a notable reduction in the total harmonic distortion of the output voltage.

When comparing multi-dimensional performance metrics, the fusion control strategy exhibits parameter adaptability. Sensitivity analysis confirms that, during load mutation simulation experiments, the voltage dynamic recovery time of the fusion strategy is comparable to that of traditional control methods, while the tracking error remains within a minimal range.

In summary, the fusion control scheme achieves rapid response, precise error tracking, and robust disturbance rejection through the nonlinear mapping of dynamic weight factors. Compared to single SMC or traditional dual closed-loop control, this approach provides a theoretically rigorous and practically viable solution for power quality control in high-performance inverters.

5. References

[1] R. Islam, S. M. S. H. Rafin, and O. A. Mohammed, “Comprehensive review of power electronic converters in electric vehicle applications,” Forecasting, vol. 5, no. 1, pp. 22-80, 2022. doi: 10.3390/forecast5010002.

[2] N. Novas, A. Alcayde, I. Robalo, F. Manzano-Agugliaro, and F. G. Montoya, “Energies and its worldwide research,” Energies, vol. 13, no. 24, p. 6700, 2020. doi: 10.3390/en13246700.

[3] H. Lin and Y. Zhang, “Strategic environmental assessment with the penetration of electric vehicles in transport network,” Environ Model Assess, vol. 25, no. 4, pp. 493-503, 2020. doi: 10.1007/s10666-020-09691-0.

[4] M. Afkar, R. Gavagsaz-Ghoachani, M. Phattanasak, and S. Pierfederici, “Voltage-balancing of two controllers for a DC-DC converter-based DC microgrid with experimental verification,” Math Comput Simul, vol. 221, pp. 159-179, 2024. doi: 10.1016/j.matcom.2024.02.019.

[5] H. Abouobaida, L. de Oliveira-Assis, E. P. P. Soares-Ramos, H. Mahmoudi, J. M. Guerrero, and M. Jamil, “Energy management and control strategy of DC microgrid based hybrid storage system,” Simul Model Pract Theory, vol. 124, p. 102726, 2023. doi: 10.1016/j.simpat.2023.102726.

[6] G. D. Oliveira and L. C. Dias, “The potential learning effect of a MCDA approach on consumer preferences for alternative fuel vehicles,” Ann Oper Res, vol. 293, no. 2, pp. 767-787, 2020. doi: 10.1007/s10479-020-03584-x.

[7] N. G. Valencia Pavón, A. Aguila Téllez, J. Rojas Urbano, V. Taramuel Obando, and E. Guanga, “Evaluation of an infinite-level inverter operation powered by a DC–DC converter in open and closed loop,” Energies, vol. 17, no. 22, p. 5593, 2024. doi: 10.3390/en17225593.

[8] M. Venkatesan et al., “A review of compensation topologies and control techniques of bidirectional wireless power transfer systems for electric vehicle applications,” Energies, vol. 15, no. 20, p. 7816, 2022. doi: 10.3390/en15207816.

[9] H. Ataullah et al., “Analysis of the dual active bridge-based DC-DC converter topologies, high-frequency transformer, and control techniques,” Energies, vol. 15, no. 23, p. 8944, 2022. doi: 10.3390/en15238944.

[10] Md. A. Hossain, Md. R. Islam, Md. A. Hossain, and M. J. Hossain, “Control strategy review for hydrogen-renewable energy power system,” J Energy Storage, vol. 72, p. 108170, 2023. doi: 10.1016/j.est.2023.108170.

[11] S. B. Hamed, M. B. Hamed, and L. Sbita, “Robust voltage control of a buck DC-DC converter: A sliding mode approach,” Energies, vol. 15, no. 17, p. 6128, 2022. doi: 10.3390/en15176128.

[12] R. Saadi, M. Y. Hammoudi, O. Kraa, M. Y. Ayad, and M. Bahri, “A robust control of a 4-leg floating interleaved boost converter for fuel cell electric vehicle application,” Math Comput Simul, 2020.

[13] J. Li, B. Pi, P. Zhou, J. Li, H. Dong, and P. Chen, “An objective holographic feedback linearization based on a sliding mode control for a buck converter with a constant power load,” Electronics, vol. 12, no. 18, p. 3976, 2023. doi: 10.3390/electronics12183976.

[14] Y. Yin, J. Mao, and R. Liu, “Multivariable-feedback sliding-mode control of bidirectional DC/DC converter in DC microgrid for improved stability with dynamic constant power load,” Electronics, vol. 11, no. 21, p. 3455, 2022. doi: 10.3390/electronics11213455.

[15] L. Wang, W. Luo, and D. Huang, “Research on automotive bidirectional CLLC resonant converters based on high-order sliding mode control,” Electronics, vol. 11, no. 18, p. 2874, 2022. doi: 10.3390/electronics11182874.

[16] L. Xu et al., “Sliding mode control for pulsed load power supply converters in DC shipboard microgrids,” Int J Electr Power Energy Syst, vol. 151, p. 109118, 2023. doi: 10.1016/j.ijepes.2023.109118.

[17] K. Ahmed, I. Hussain, M. Seyedmahmoudian, A. Stojcevski, and S. Mekhilef, “Voltage stability and power sharing control of distributed generation units in DC microgrids,” Energies, vol. 16, no. 20, p. 7038, 2023. doi: 10.3390/en16207038.

[18] G. Luo et al., “ROV trajectory tracking control based on disturbance observer and combinatorial reaching law of sliding mode,” Ocean Eng, vol. 304, p. 117744, 2024. doi: 10.1016/j.oceaneng.2024.117744.

[19] J.-H. Xu et al., “Sliding mode – Extended state observer control strategy to improve energy transfer of PEMFC connected DC-DC boost converter system,” Sustain Energy Technol Assess, vol. 63, p. 103654, 2024. doi: 10.1016/j.seta.2024.103654.

[20] M. I. Azeez, A. M. M. Abdelhaleem, S. Elnaggar, K. A. F. Moustafa, and K. R. Atia, “Optimized sliding mode controller for trajectory tracking of flexible joints three-link manipulator with noise in input and output,” Sci Rep, vol. 13, no. 1, 2023. doi: 10.1038/s41598-023-38855-7.

[21] Diouf, B. Belzile, M. Saad, and D. St-Onge, “Spherical rolling robots—Design, modeling, and control: A

systematic literature review," Robot Auton Syst, vol. 175, p. 104657, 2024. doi: 10.1016/j.robot.2024.104657.